JOURNAL OF COMPUTATIONAL PHYSICS 18, 46–65 (1975)

Flow Past Impulsively Started Bodies Using Green's Functions

P. K. G. PANIKKER

Fluor Pioneer Incorporated, Chicago, Illinois

AND

Z. LAVAN

Illinois Institute of Technology, Chicago, Illinois

Received August 21, 1974; revised January 22, 1975

Numerical solutions are obtained for viscous incompressible flow over an impulsively started cylinder and a 2:1 ellipse at an angle of attack of 20°. The Navier–Stokes equations with vorticity and stream function as variables are solved using a combination of finite differences and Green's function. The Reynolds numbers are 500 and 200 for the cylinder and ellipse respectively, and computations are continued up to a dimensionless time of 1.5. For the flow over an ellipse the lift force as well as the drag are initially very large and then rapidly decay. The rear stagnation point gradually moves down and separation occurs at $t \sim 1.1$. Recent experimental studies by Taneda for flow at the same geometry indeed show large values of lift following the initial motion and gradual downward movement of the rear stagnation point.

1. INTRODUCTION

In the present work we seek a solution to the flow past an impulsively started circular cylinder and an ellipse at an angle of attack. A computation scheme using Green's functions is formulated and used. This relaxes the need to specify faraway boundary conditions and reduces the field of computation. In this method Poisson's stream function equation is solved by integral relations in a manner similar to that used by Thompson, Shanks, and Wu [1], who solved the time dependent flow over a rectangular slab at an angle of attack.

Following the impulsive start, the fluid in contact with the body is at rest whereas the adjacent layers slip past the surface. The vorticity generated at the surface is first diffused and later it is simultaneously diffused and convected. Hence, a boundary layer grows on the surface, the rate of growth is initially very large, and

it diminishes with time. In the region of adverse pressure gradient, the forward stream eventually separates from the surface; and as time increases, the point of separation moves upstream resulting in a distinct separated region.

Analytical solutions to such impulsively started flows often resort to perturbation schemes. For a circular cylinder Blasius [2], Goldstein and Rosenhead [3], and Watson [4] obtained analytical solutions as an expansion in time assuming the pressure distribution to be that of the steady potential flow over the original body. They predict correctly the onset of separation and the viscous drag even for moderate Reynolds numbers. However, their argument that the pressure drag is zero would be correct only in the limit as Reynolds number goes to infinity for $t \neq 0$. Proudman and Johnson [5] solved the unsteady Navier–Stokes equation in the neighborhood of the rear stagnation point of an impulsively started circular cylinder. The analysis starts with the solution of Blasius [2] and results that are valid for attached wakes are obtained. They predict that the wake length grows exponentially with time and is proportional to $R_e^{-1/2}$. Wang [6, 7] used an inner–outer expansion to solve the unsteady incompressible Navier–Stokes equations for the flow past an impulsively started circular cylinder. He obtained a pressure drag that is proportional to $t^{-1/2}$. Collins and Dennis [8] extended Wang's approximation to larger time and lower Reynolds numbers. In a second paper Collins and Dennis [9] utilize an expansion in sin $n\theta$ for the vorticity and stream function. They use the unsteady boundary layer transformation to obtain solutions at small time and later switch to the original variables.

Perhaps the earliest numerical solution of unsteady incompressible Navier-Stokes equations for the flow past an impulsively started circular cylinder is that of Payne [10]. He uses an explicit time difference formula for the vorticity equation, and velocities are calculated directly from vorticity. Drag is calculated by the rate of decrease of momentum of the fluid. The unsteady flow over a cylinder was also solved numerically by Son and Hanratty [11], Kawaguti and Jain [12], Thoman and Szewczyk [13], and Jain and Rao [14].

Howarth [15] discusses the development of circulation around a thin elliptic cylinder and predicts that no lift occurs up to the time of separation. Wang [16], on the other hand, finds that the lift continuously increases from an initial value of zero. Dennis and Staniforth [17] considered the flow past an impulsively started body at an angle of attack using boundary layer equations and a spatial transformation that stretches time. They solved the flow past a cylinder for various Reynolds numbers as a test problem.

Numerical solutions of laminar flow past elliptic cylinders at various angles of attack were obtained by Lugt and Haussling [18] for Reynolds numbers of 10 to 200 and angles of attack of 45° and 90°. Mehta and Lavan [19] have solved numerically the problem of an impulsively started symmetric 9 % thick airfoil at an angle of attack of 15° and Reynolds number of 1000. In the last two studies the

initial lift is very high. Telionis and Tsahalis [20] studied separation over impulsively started circular and elliptical cylinders using boundary layer equations.

An experimental study of the flow over a circular cylinder started impulsively from rest was carried out by Schwabe [21] for Reynolds number of 560. Honji and Taneda [22] studied the development of symmetrical unsteady vortices behind impulsively started circular cylinders for Reynolds numbers ranging from 31 to 1700. Recently Taneda [23] studied experimentally the flow over a 2 : 1 ellipse following an impulsively started motion. He reports very high initial lift values and a gradual downward movement of the rear stagnation point.

2. Mathematical Formulation

The study deals with incompressible viscous laminar flow over a circular cylinder and an ellipse at an angle of attack. The mathematical development, however, is general to permit all two-dimensional bodies that can be generated by a Joukowski transformation. The governing equations are the vorticity transport and stream function equations. In cartesian coordinates ξ, η (see Fig. 1) the nondimensional equations are

$$(\partial\omega/\partial t) + u(\partial\omega/\partial\xi) + v(\partial\omega/\partial\eta) = (l/R_e)[(\partial^2\omega/\partial\xi^2) + (\partial^2\omega/\partial\eta^2)], \tag{1}$$

$$(\partial^2\Psi/\partial\xi^2) + (\partial^2\Psi/\partial\eta^2) = -\omega, \tag{2}$$

where

$$u = \partial\Psi/\partial\eta, \qquad v = -\partial\Psi/\partial\xi. \tag{3}$$

The reference velocity used is U_∞, and the reference length is the mean of the semi-major, a, and minor, b, axes of the ellipse, i.e. $(a + b)/2$. Hence the nondimensional chord length and time are $l = 2a/[(a + b)/2]$, and $t = \bar{t}U_\infty/[(a + b)/2]$ (where $\bar{t}$ is dimensional time). The Reynolds number is given by $R_e = 2aU_\infty/\nu$.

The uniform flow U_∞ makes an angle, Λ, with the direction of the chord, ξ. In order to avoid large numerical values of the stream function at large distances the uniform flow is subtracted out. The resulting difference stream function, ψ, is defined by

$$\psi = \Psi - \eta\cos\Lambda + \xi\sin\Lambda \tag{4}$$

and Eqs. (1), (2) become

$$\frac{\partial\omega}{\partial t} + \left(\frac{\partial\psi}{\partial\eta} + \cos\Lambda\right)\frac{\partial\omega}{\partial\xi} + \left(-\frac{\partial\psi}{\partial\xi} + \sin\Lambda\right)\frac{\partial\omega}{\partial\eta} = \frac{l}{R_e}\left(\frac{\partial^2\omega}{\partial\xi^2} + \frac{\partial^2\omega}{\partial\eta^2}\right), \tag{5}$$

$$(\partial^2\psi/\partial\xi^2) + (\partial^2\psi/\partial\eta) = -\omega. \tag{6}$$

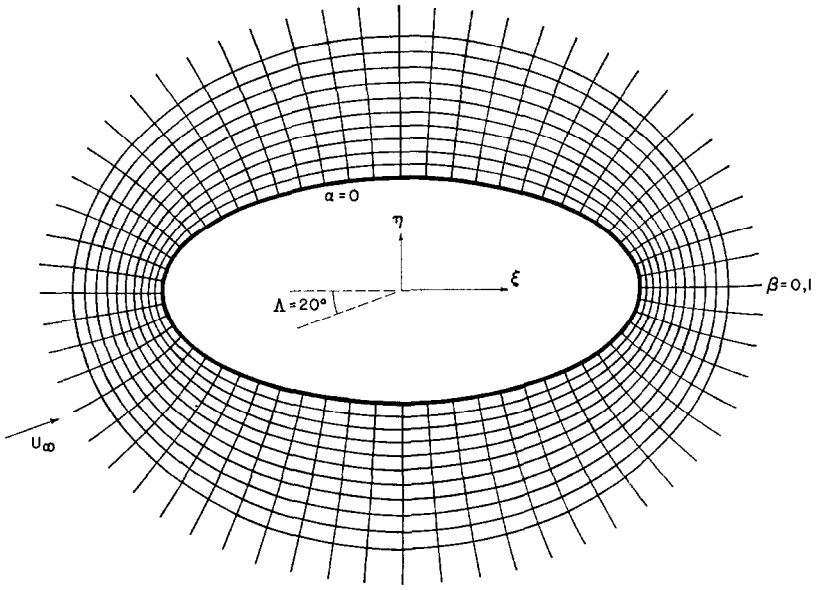

FIG. 1. Schematic of grid over a 2:1 ellipse at 20° angle of attack.

The ellipse is obtained from a circle hereafter called the circle plane through a Joukowski transformation

$$\zeta = Z + (C/Z), \tag{7}$$

where $Z = X + iY$ and $\zeta = \xi + i\eta$. Since the transformation is conformal the Cauchy–Riemann equations give

$$\partial X/\partial \xi = \partial Y/\partial \eta = A, \qquad -\partial X/\partial \eta = \partial Y/\partial \xi = B, \tag{8}$$

and Eqs. (5, 6) become in the circle plane

$$\frac{\partial \omega}{\partial t} + (A \cos \Lambda - B \sin \Lambda)\frac{\partial \omega}{\partial X} + (B \cos \Lambda + A \sin \Lambda)\frac{\partial \omega}{\partial Y} + (A^2 + B^2)\left(\frac{\partial \psi}{\partial Y}\frac{\partial \omega}{\partial X} - \frac{\partial \psi}{\partial X}\frac{\partial \omega}{\partial Y}\right) = (A^2 + B^2)\frac{l}{R_e}\left(\frac{\partial^2 \omega}{\partial X^2} + \frac{\partial^2 \omega}{\partial Y^2}\right), \tag{9}$$

$$(\partial^2 \psi/\partial X^2) + (\partial^2 \psi/\partial Y^2) = -\omega/(A^2 + B^2). \tag{10}$$

At the Reynolds numbers that we will consider we expect large gradients of vorticity close to the surface. Equations (9), (10) are therefore transformed into the working plane, w, using

$$w = \alpha + i\beta = (1/2\pi)\ln(X + iY) \tag{11}$$

in order to stretch the normal coordinate near the surface. The Cauchy–Riemann equations are

$$C = \partial\alpha/\partial X = \partial\beta/\partial Y, \qquad D = -\partial\alpha/\partial Y = \partial\beta/\partial X, \tag{12}$$

and the final equations are

$$\begin{aligned}\frac{\partial\omega}{\partial t} &+ (AC\cos\Lambda - BC\sin\Lambda - BD\cos\Lambda - AD\sin\Lambda)\frac{\partial\omega}{\partial\alpha} \\ &+ (AD\cos\Lambda - BD\sin\Lambda + BC\cos\Lambda + AC\sin\Lambda)\frac{\partial\omega}{\partial\beta} \\ &+ (A^2 + B^2)(C^2 + D^2)\left(\frac{\partial\psi}{\partial\beta}\frac{\partial\omega}{\partial\alpha} - \frac{\partial\psi}{\partial\alpha}\frac{\partial\omega}{\partial\beta}\right) \\ &= \frac{l}{R_e}(A^2 + B^2)(C^2 + D^2)\left(\frac{\partial^2\omega}{\partial\alpha^2} + \frac{\partial^2\omega}{\partial\beta^2}\right)\end{aligned} \tag{13}$$

and

$$(\partial^2\psi/\partial\alpha^2) + (\partial^2\psi/\partial\beta^2) + \omega/[(A^2 + B^2)(C^2 + D^2)] = 0. \tag{14}$$

Initially (following the impulsive start) the vorticity is zero everywhere and the stream function is given by the potential flow solution. (See for example Milne-Thompson [24].) Hence at $t = 0$,

$$\psi = \frac{(c-1)\sin(2\pi\beta)\cos\Lambda + (c+1)\cos(2\pi\beta)\sin\Lambda}{e^{2\pi\alpha}}. \tag{15}$$

On the surface of the body the no-slip condition holds at all times, i.e.

$$\Psi = \partial\Psi/\partial\alpha = 0 \tag{16}$$

At the outer boundary the vorticity is zero. The need for an outer boundary condition on stream function depends on the solution method: When Eq. (14) is solved by relaxation, an outer boundary condition on ψ must be given. When the Green function formulation is used no condition on ψ is required. Since the Green function for Poisson's equation is known for the interior of a circle, we transform Eq. (10) to the interior of a circle through

$$\Omega = 1/Z = \rho e^{i\theta} = \tau + i\sigma \tag{17}$$

and obtain

$$\nabla^2\psi = -\omega[(1/\rho^4) + c^2 - (2c/\rho^2)\cos 2\theta] \equiv -f(\rho, \theta), \tag{18}$$

where f is a known function at the interior points of the unit circle, $\rho = 1$. The boundary condition on the surface is $\Psi = 0$ or

$$\psi = -(c - 1) \sin\theta \cos\Lambda + (c + 1) \cos\theta \sin\Lambda \equiv g(\theta). \tag{19}$$

The solution of Eq. (18) can be split as

$$\psi = \psi_1 + \psi_2 , \tag{20}$$

where ψ_1 is a solution to

$$\nabla^2\psi_1 = 0 \tag{21}$$

(see Eq. (15)) with ψ_1 on the boundary being $g(\theta)$. A closed form solution for ψ_2 is obtained from

$$\psi_2(\hat{\Omega}) = \frac{1}{2\pi}\int_{|\Omega|<1} f(\rho, \theta) \ln\left(\frac{1 - \bar{\Omega}\hat{\Omega}}{\hat{\Omega} - \Omega}\right) dA \tag{22}$$

given by Kantarovich and Krylov [25]. In this equation $\bar{\Omega}$ is the complex conjugate of Ω and each point value of $\psi_2(\hat{\Omega})$ is obtained by integration over the entire area. Note that ψ_2 is zero on the surface.

3. Numerical Method

The vorticity Eq. (13) is solved in the w plane taking equal increments in α and β ($\Delta\alpha \neq \Delta\beta$). The number of points in the β direction was always 80. However, as time progresses and vorticity spreads, additional entire α lines (not points) are added in the integration. (At $t = 1.5$, 62 α lines were used.) The time increment was first 10^{-4} and was increased to 10^{-2} at $t = 1.5$.

The vorticity equation is numerically advanced in time using a forward explicit marching method. Next the stream function equation is solved in the entire field, (as will be explained later). The value of vorticity at the surface for the new time is obtained using Woods' [26] three-point method.

$$\omega_{1,j} = -\left[\frac{6\psi_{2,j}}{(\Delta\alpha)^3} + \frac{\omega_{2,j}}{\Delta\alpha\, H_{1,j}}\right] \Big/ \left[\frac{2}{H_{1,j}\,\Delta\alpha} + 16\pi^3(1 - c^2)\right], \tag{23}$$

where

$$H_{1,j} = 1/\{4\pi^2[1 - 2c\cos(4\pi\beta) + c^2]\}.$$

Here, i and j are defined by $\alpha = (i - 1)\,\Delta\alpha$ and $\beta = (j - 1)\,\Delta\beta$. Hence, $i = 1$ denotes the surface and 2 denotes the grid point next to the surface.

The method for computing vorticity is well known and no further details will be given here. (See for example Refs. [12, 13].) A detailed description of the way ψ is calculated is given next.

We expand $\ln | \hat{\Omega} - \Omega |$, in an appropriate power series. For values of Ω between zero and $\hat{\Omega}$ we use

$$\ln | \hat{\rho} e^{i\hat{\theta}} - \rho e^{i\theta} | = \ln \hat{\rho} - \sum_{n=1}^{\infty} \frac{1}{n} \frac{\rho^n}{\hat{\rho}^n} \cos n(\theta - \hat{\theta}). \tag{24}$$

For values of Ω between $\hat{\Omega}$ and 1 we take

$$\ln | \hat{\rho} e^{i\hat{\theta}} - \rho e^{i\theta} | = \ln \rho - \sum_{n=1}^{\infty} \frac{1}{n} \frac{\hat{\rho}^n}{\rho^n} \cos n(\hat{\theta} - \theta). \tag{25}$$

Hence the series solution for ψ_2 is obtained in the form

$$\begin{aligned} 2\pi\psi_2 = & \int_0^{2\pi} \int_0^{\hat{\rho}} \left[-\ln \hat{\rho} + \sum_{n=1}^{\infty} \frac{1}{n} \frac{\rho^n}{\hat{\rho}^n} \cos n(\hat{\theta} - \theta) \right] f\rho \, d\rho \, d\theta \\ & + \int_0^{2\pi} \int_{\hat{\rho}}^{1} \left[-\ln \rho + \sum_{n=1}^{\infty} \frac{1}{n} \frac{\hat{\rho}^n}{\rho^n} \cos n(\hat{\theta} - \theta) \right] f\rho \, d\rho \, d\theta \\ & - \int_0^{2\pi} \int_0^{1} \left[\sum_{n=1}^{\infty} \frac{1}{n} \rho^n \hat{\rho}^n \cos n(\hat{\theta} - \theta) \right] f\rho \, d\rho \, d\theta \end{aligned} \tag{26}$$

or

$$2\pi\psi_2 = I_1 + I_2 + I_3 . \tag{27}$$

Since ω is a periodic function of θ, Green's function is obtained as a trigonometric series, i.e., ω at fixed ρ is expanded in a Fourier series that can be integrated over the variable θ making use of the orthogonal properties. We obtain

$$\begin{aligned} I_1 = \pi \Big[& \int_0^{\hat{\rho}} - \ln \hat{\rho} \left[\left(c^2 + \frac{1}{\rho^4} \right) a_0 - \frac{2c}{\rho^2} a_2 \right] \rho \, d\rho \\ & + \frac{\cos \hat{\theta}}{\hat{\rho}} \int_0^{\hat{\rho}} \left[\left(c^2 + \frac{1}{\rho^4} \right) a_1 \rho - \frac{c}{\rho^2} \rho (a_1 + a_3) \right] \rho \, d\rho \\ & + \frac{\cos 2\hat{\theta}}{2\hat{\rho}^2} \int_0^{\hat{\rho}} \left[\left(c^2 + \frac{1}{\rho^4} \right) a_2 \rho^2 - \frac{c}{\rho^2} \rho^2 (a_0 + a_4) \right] \rho \, d\rho \\ & + \frac{\cos 3\hat{\theta}}{3\hat{\rho}^3} \int_0^{\hat{\rho}} \left[\left(c^2 + \frac{1}{\rho^4} \right) a_3 \rho^3 - \frac{c}{\rho^2} \rho^3 (a_1 + a_5) \right] \rho \, d\rho \\ & + \text{----------} \\ & + \frac{\sin \hat{\theta}}{\hat{\rho}} \int_0^{\hat{\rho}} \left[\left(c^2 + \frac{1}{\rho^4} \right) b_1 \rho - \frac{c}{\rho^2} \rho (-b_1 + b_3) \right] \rho \, d\rho \\ & + \frac{\sin 2\hat{\theta}}{2\hat{\rho}^2} \int_0^{\hat{\rho}} \left[\left(c^2 + \frac{1}{\rho^4} \right) b_2 \rho^2 - \frac{c}{\rho^2} \rho^2 (0 + b_4) \right] \rho \, d\rho \\ & + \frac{\sin 3\hat{\theta}}{3\hat{\rho}^3} \int_0^{\hat{\rho}} \left[\left(c^2 + \frac{1}{\rho^4} \right) b_3 \rho^3 - \frac{c}{\rho^2} \rho^3 (b_1 + b_5) \right] \rho \, d\rho + \cdots \Big]. \end{aligned} \tag{28}$$

$$I_2 = \pi \Big[\int_{\hat\rho}^{1} \Big[-\ln\rho \Big[\Big(c^2 + \frac{1}{\rho^4}\Big) a_0 - \frac{2c}{\rho^2} a_2\Big] \rho\, d\rho$$

$$+ \hat\rho \cos\hat\theta \int_{\hat\rho}^{1} \Big[\Big(c^2 + \frac{1}{\rho^4}\Big) \frac{a_1}{\rho} - \frac{c}{\rho^2} \frac{(a_1 + a_3)}{\rho}\Big] \rho\, d\rho$$

$$+ \frac{\hat\rho^2 \cos 2\hat\theta}{2} \int_{\hat\rho}^{1} \Big[\Big(c^2 + \frac{1}{\rho^4}\Big) \frac{a_2}{\rho^2} - \frac{c}{\rho^2} \frac{(a_0 + a_4)}{\rho^2}\Big] \rho\, d\rho$$

$$+ \frac{\hat\rho^3 \cos 3\hat\theta}{3} \int_{\hat\rho}^{1} \Big[\Big(c^2 + \frac{1}{\rho^4}\Big) \frac{a_3}{\rho^3} - \frac{c}{\rho^2} \frac{(a_1 + a_5)}{\rho^3}\Big] \rho\, d\rho$$

$$+ \text{----} \quad \text{----------}$$

$$+ \hat\rho \sin\hat\theta \int_{\hat\rho}^{1} \Big[\Big(c^2 + \frac{1}{\rho^4}\Big) \frac{b_1}{\rho} - \frac{c}{\rho^2} \frac{(-b_1 + b_3)}{\rho}\Big] \rho\, d\rho$$

$$+ \frac{\hat\rho^2 \sin 2\hat\theta}{2} \int_{\hat\rho}^{1} \Big[\Big(c^2 + \frac{1}{\rho^4}\Big) \frac{b_2}{\rho^2} - \frac{c}{\rho^2} \frac{(0 + b_4)}{\rho^2}\Big] \rho\, d\rho$$

$$+ \frac{\hat\rho^3 \sin 3\hat\theta}{3} \int_{\hat\rho}^{1} \Big[\Big(c^2 + \frac{1}{\rho^4}\Big) \frac{b_3}{\rho^3} - \frac{c}{\rho^2} \frac{(b_1 + b_5)}{\rho^3}\Big] \rho\, d\rho$$

$$+ \text{----------}\Big]. \tag{29}$$

$$I_3 = \pi \Big[\cos\hat\theta\hat\rho \int_{0}^{1} \Big[\Big(c^2 + \frac{1}{\rho^4}\Big) a_1\rho - \frac{c}{\rho^2} (a_1 + a_3)\, \rho\Big] \rho\, d\rho$$

$$+ \frac{\cos 2\hat\theta\hat\rho^2}{2} \int_{0}^{1} \Big[\Big(c^2 + \frac{1}{\rho^4}\Big) a_2\rho^2 - \frac{c}{\rho^2} (a_0 + a_4)\, \rho^2\Big] \rho\, d\rho$$

$$+ \frac{\cos 3\hat\theta\hat\rho^3}{3} \int_{0}^{1} \Big[\Big(c^2 + \frac{1}{\rho^4}\Big) a_3\rho^3 - \frac{c}{\rho^2} (a_1 + a_5)\, \rho^3\Big] \rho\, d\rho$$

$$+ \text{----------}$$

$$+ \sin\hat\theta\hat\rho \int_{0}^{1} \Big[\Big(c^2 + \frac{1}{\rho^4}\Big) b_1\rho - \frac{c}{\rho^2} (-b_1 + b_3)\, \rho\Big] \rho\, d\rho$$

$$+ \frac{\sin 2\hat\theta\hat\rho^2}{2} \int_{0}^{1} \Big[\Big(c^2 + \frac{1}{\rho^4}\Big) b_2\rho - \frac{c}{\rho^2} (0 + b_4)\, \rho^2\Big] \rho\, d\rho$$

$$+ \frac{\sin 3\hat\theta\hat\rho^3}{3} \int_{0}^{1} \Big[\Big(c^2 + \frac{1}{\rho^4}\Big) b_3\rho - \frac{c}{\rho^2} (b_1 + b_5)\, \rho^3\Big] \rho\, d\rho$$

$$+ \text{----------}\Big]. \tag{30}$$

Since the values of the Fourier coefficients (the a's and b's) are known functions of α we replace ρ by α using $\rho = e^{-2\pi\alpha}$. The integration is then carried out to an accuracy of $(\Delta\alpha)^5$, yielding ψ_2. Equation (15) gives the solution to ψ_1 and $\psi = \psi_1 + \psi_2$ as stated earlier.

For the purpose of comparison, a solution for the flow over an ellipse was obtained also by direct point-successive over-relaxation. The flow over an impulsively started cylinder is computed using Green's function only since comparison can be made with solutions of others.

After the velocity and vorticity fields are computed the pressure on the surface is calculated from

$$P - P_0 = \frac{2l}{R_e} \int_0^\beta \frac{\partial \omega}{\partial \alpha}\, d\beta, \tag{31}$$

where P_0 is an arbitrarily assigned value at the trailing edge. We do not enforce the condition that $\int_0^1 (\partial\omega/\partial\alpha)\, d\beta = 0$. Therefore, the numerically computed values of pressure using Eq. (31) need not be single valued. We judge the quality of the calculated pressure field by the proximity of $\int_0^1 (\partial\omega/\partial\alpha)\, d\beta$ to zero. See further discussion in Section 4.

The force coefficients in ξ and η directions are obtained by contour integration on the surface.

$$C_{F\eta} = \oint (P\, d\xi/l), \tag{32}$$

$$C_{F\xi} = \oint (P\, d\eta/l), \tag{33}$$

$$C_{S\xi} = 2 \oint (\omega_s\, d\xi/R_e), \tag{34}$$

$$C_{S\eta} = 2 \oint (\omega_s\, d\eta/R_e), \tag{35}$$

where the first subscript denotes contribution due to pressure or shear and the second subscript indicates the direction of the force.

The coefficients of lift and drag are, therefore,

$$C_{DP} = C_{F\eta} \sin \Lambda + C_{F\xi} \cos \Lambda, \tag{36}$$

$$C_{DS} = C_{S\xi} \cos \Lambda - C_{S\eta} \sin \Lambda, \tag{37}$$

$$C_{LP} = C_{F\eta} \cos \Lambda - C_{F\xi} \sin \Lambda, \tag{38}$$

$$C_{LS} = C_{S\xi} \sin \Lambda + C_{S\eta} \cos \Lambda. \tag{39}$$

The last term, (shear contribution to lift), for $\Lambda = 20°$ is negligible.

4. Discussion of Results

A. *Flow over a Cylinder*

A solution was obtained for flow over an impulsively started circular cylinder at a Reynolds number of 500. The Green function method only was used and calculations were carried out up to $t = 1.5$. The computed surface vorticities, ω_s, at $t = 0.3$ and 1.0 are shown in Figs. 2 and 3, where they are compared with those

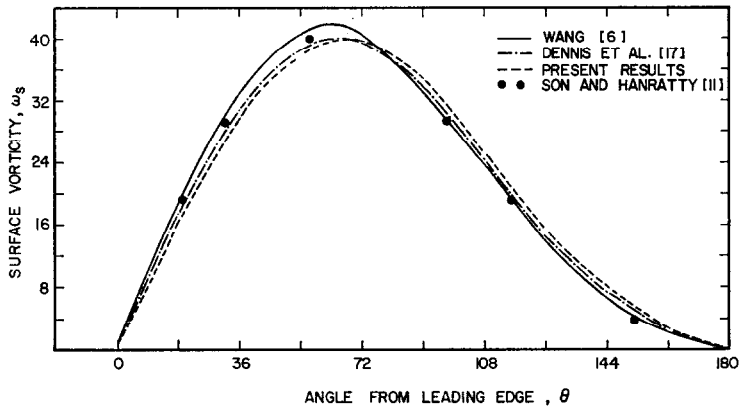

FIG. 2. Surface vorticity on a circular cylinder at $t = 0.3$.

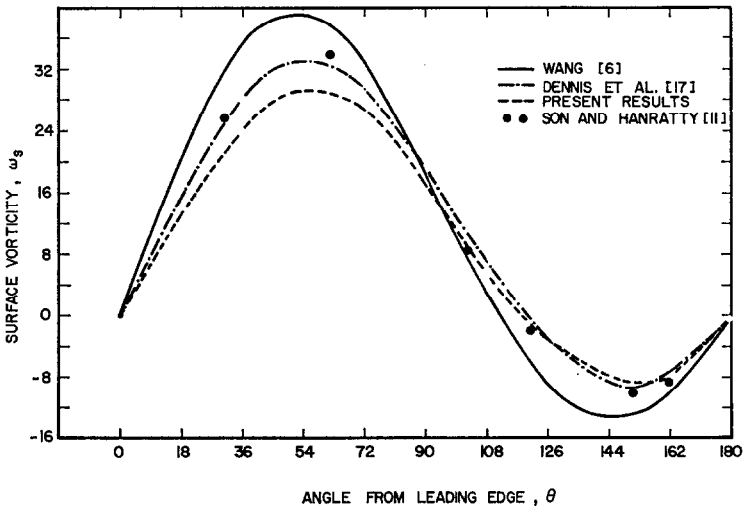

FIG. 3. Surface vorticity on a circular cylinder at $t = 1.0$.

of Dennis and Staniforth [17], Wang [6], and Son and Hanratty [11]. The surface vorticity obtained from Wang's solution in our variables is

$$\omega_s = \frac{2^{1/2} \sin \phi (R_e)^{1/2}}{(\pi t)^{1/2}} \left[1 + \frac{(\pi t)^{1/2}}{(2R_e)^{1/2}} + 2t \cos \phi \left(1 + \frac{4}{3\pi}\right)\right]. \tag{40}$$

Figure 2 shows that the agreement between the four studies is good at $t = 0.3$ where the flow did not yet separate.

Figure 3 shows that at $t = 1.0$ the surface vorticities of the four solutions do not retain the close agreement. Wang's solution exhibits the largest discrepancy, probably since his time expansion is already relatively inaccurate at this time when separation is present.

Separation starts at $t_s = 0.37$ according to our calculations. Dennis and Staniforth [17] and Collins and Dennis [9] give $t_s = 0.39$; Thomas and Szewczyk [13] state that $t_s \sim 0.35$; Collins and Dennis [8] report $t_s \sim 0.41$; while Wang [6] finds 0.35. The classical analytical boundary layer solution of Blasius [2] gives the

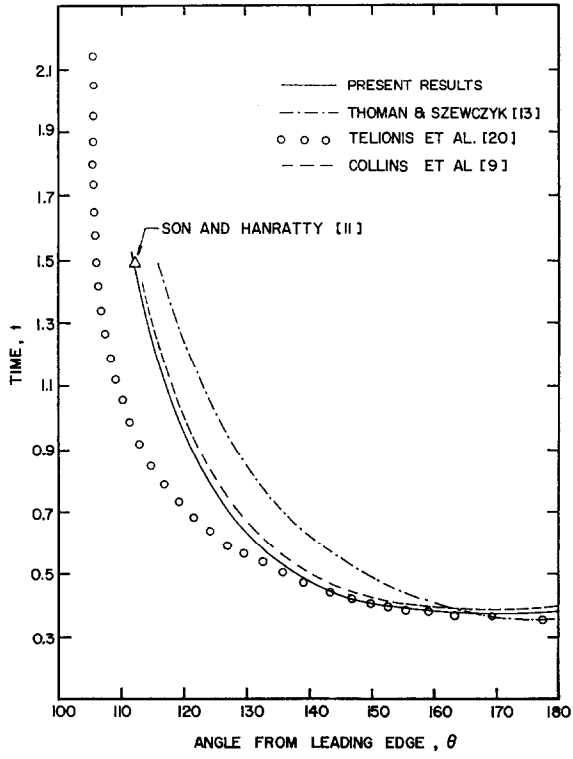

FIG. 4. Position of the point of vanishing shear, θ_s on a circular cylinder versus time.

separation time for the limiting case of $R_e \to \infty$ as $t_s = 0.35$. The second approximation of Goldstein and Rosenhead [3] gives $t_s = 0.3195$. Collins and Dennis [8] show that t_s remains 0.322 when higher approximations (up to seventh) are considered. While it is expected that for finite R_e, t_s should increase, it is not clear yet exactly how t_s varies with R_e.

Figure 4 shows the location of the point of vanishing shear, θ_s, on a circular cylinder as a function of time. Our computed values of θ_s are very close to those of Collins and Dennis [9] and are in agreement with Son and Hanratty [11] at $t = 1.5$. (We were unable to compare at smaller t.) The results of Thoman and Szewczyk [13] show a slower movement of θ_s for $R_e = 600$. (For $R_e = 500$ the movement would be even slower.) We also show in Figure 4 boundary layer calculations of Telionis and Tsahalis [20], which show an asymptotic solution for $R_e \to \infty$. Clearly no comparison of flow with $R_e = 500$ should be made with this solution.

Figure 5 shows our computed wake length as a function of time and the experimental values obtained by Honji and Taneda [22]. Although the two time domains do not overlap the sets of results clearly show the same trend.

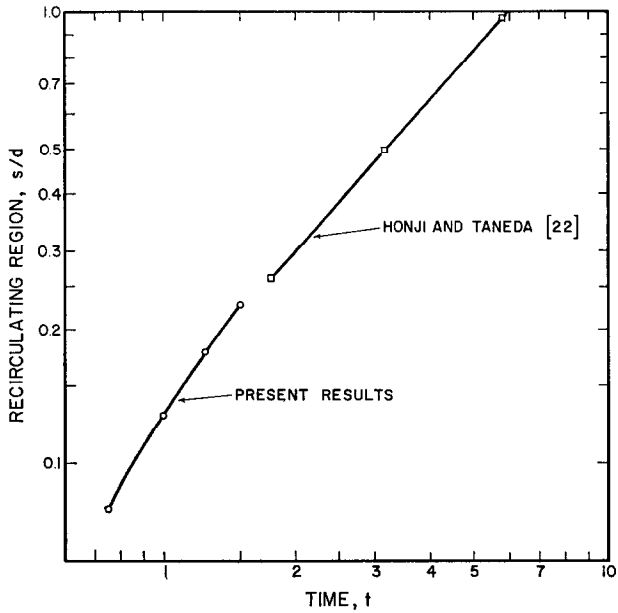

FIG. 5. Time variation of drag coefficients.

Figure 6 shows the variation of the drag coefficients with time. The skin friction drag, C_{DS}, decreases monotonically. The initial large value is due to the discontinuity of vorticity on the surface following the impulsive start. The theoretical

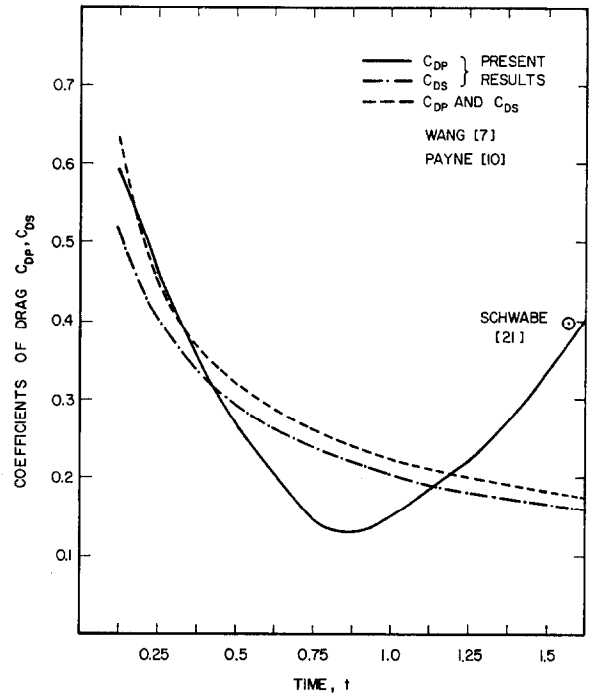

FIG. 6. Length of recirculating region behind a circular cylinder as function of time.

analyses of Blasius [2] and Goldstein and Rosenhead [3] give the friction drag coefficient as

$$C_{DS} = 2(2\pi)^{1/2}/(R_e t)^{1/2}. \tag{41}$$

This is the same expression obtained by Wang [7] and Payne [10]. Figure 6 shows that the agreement between our computed values and the analytical results for C_{DS} is good. The behavior of C_{DP} is much more complex. Figure 6 shows that it also is initially very large. It reaches a minimum of 0.1325 at approximately $t = 0.8$ and it then increases. The initial large values of C_{DP} are due to the unsteady nature of the flow. The subsequent increase in C_{DP} is due to the development of the separation region. Schwabe's [21] result is also shown in this figure. He obtained C_{DP} from experimental observations of the flow pattern at a Reynolds number of 560. His value of 0.4 at $t = 1.6$ agrees fairly well with our value of 0.338 at $t = 1.5$.

Goldstein and Rosenhead [3] argue that the pressure drag is zero since the variation of pressure across the thin boundary layer can be neglected, and the outer flow is the steady potential flow field. This is valid only in the limit of $R_e \to \infty$. For finite R_e, the value of $\partial P/\partial n$ (while small compared to the other terms in

the momentum equation) must be considered when calculating C_{DP}. Payne [10] calculated the value of pressure drag for small time by evaluating the rate of change of momentum in the direction of flow, x. He used the expression given by Phillips [27],

$$D_P = -\frac{d}{dt}\int_A \rho\omega y \, dA, \tag{42}$$

and the vorticity solution of Blasius [2] and obtained values of C_{DP} that tend to infinity as $t \to 0$, i.e., $C_{DP} = 2(2\pi)^{1/2}/(R_e t)^{1/2}$. Wang [7] obtained the same expression for C_{DP}. These analytical results predict that C_{DP} decreases continuously with time. The agreement with our computed results is good only until $t \sim 0.4$ where separation starts.

The large initial values of C_{DP} for flow over a cylinder were noted earlier in a number of numerical studies. Jain and Rao [14] report values of C_{DP} for Reynolds numbers ranging from 40 to 200 and for $R_e = 1000$. Kawaguti and Jain [12] give

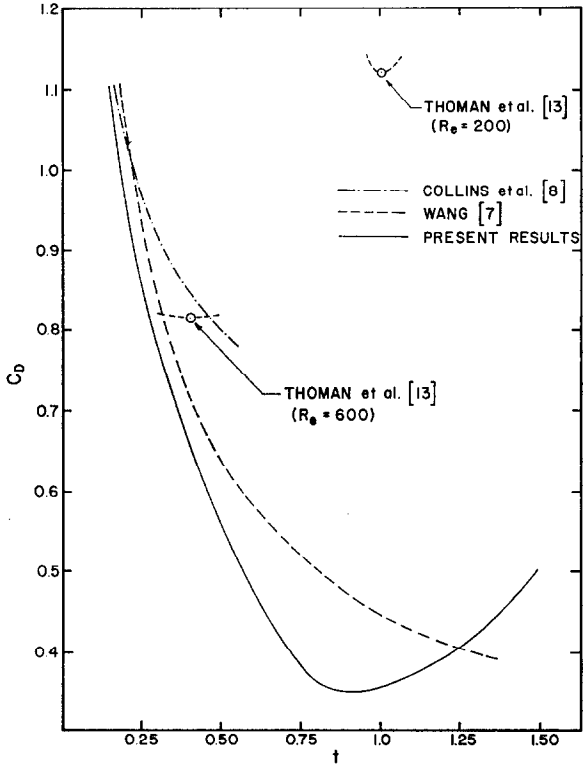

FIG. 7. Variation of C_D with time.

values for C_{DP} for $10 \leqslant R_e \leqslant 50$. The numerical studies of flow at Reynolds numbers comparable to ours [8, 9, 11, 13, 17] do not explicitly report C_{DP} although they were calculated in arriving at C_D.

Figure 7 shows the variation of the total drag C_D as a function of time. The reported values of C_D for $t < 1.5$ are very scarce. Our results agree in trend with those of Wang [7] and Collins and Dennis [8] for $t < 0.4$. The values of Thoman and Szewczyk [13] for minimum C_D at $R_e = 200$ and 600 (shown in Fig. 7) are quite different from our results.

B. *Flow over an Ellipse*

The impulsively started flow over a 2 : 1 ellipse at an angle of attack of 20° and Reynolds number of 200 (based on the major axis) was computed. Results were obtained using both the Green function method and successive overrelaxation using the same grid. The flow field is almost identical in both cases. Nevertheless, the resultant pressure fields were considerably different when these two flow fields were used.

The pressure on the surface of the ellipse is obtained from Eq. (31) with the value of zero assigned to the trailing edge. The quality of the pressure calculations is judged by the closure of the pressure value; i.e., by the proximity of P_r to zero, where

$$P_r = [P(0) - P(2\pi)]/\Delta P_{\max} \tag{43}$$

and $(\Delta P)_{\max}$ is the maximum pressure difference on the entire surface.

TABLE I

Comparison of P_r by the Two Methods

Time	Green's function	Overrelaxation
0.5	0.0493	0.2023
1.0	0.0300	0.1742
1.5	0.0652	0.2533

It can be seen from Table I that the accuracy of the pressure results when the Green function method is used is considerably better. It would, of course, be preferred if the periodicity of pressure could be enforced in the numerical formulation.[1]

Initially the rear stagnation point is at $\xi = 1.25$ and $\eta = 0.22$ (see point I in Fig. 8). As time progresses, the rear stagnation point moves toward the trailing

[1] The question of pressure periodicity was raised by one of the reviewers.

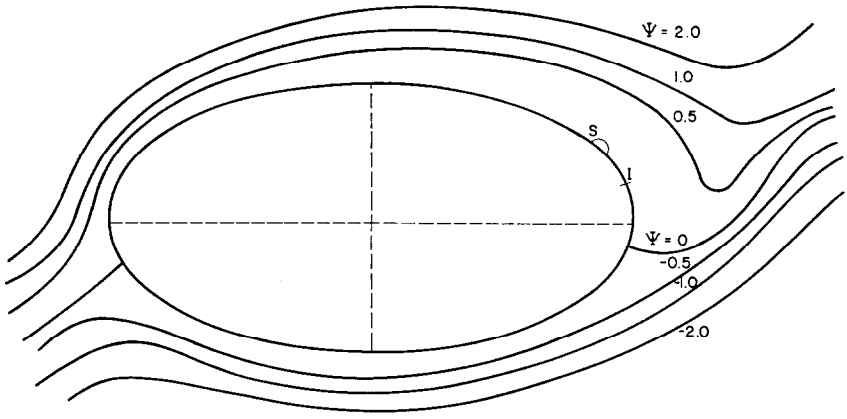

FIG. 8. Stream function contours for flow over an ellipse at $t = 1.5$.

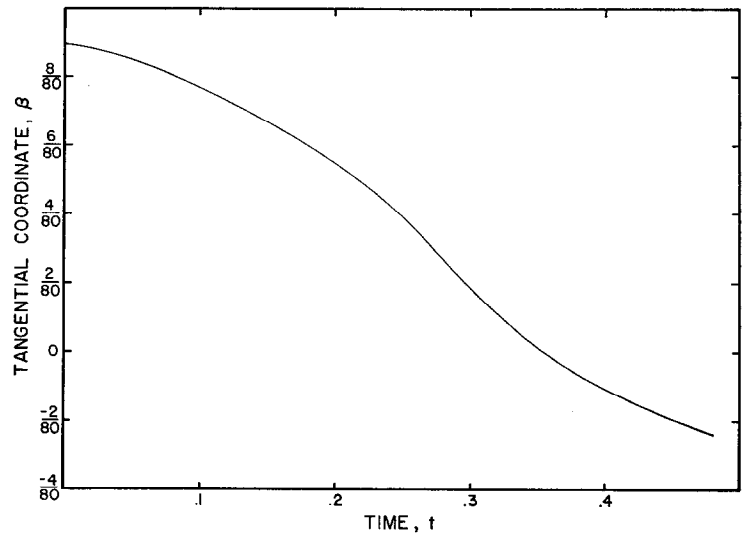

FIG. 9. Position of the point of vanishing shear on the ellipse versus time.

edge as shown in Fig. 9. The front stagnation point is nearly stationary during this period. Separation starts at $t = 1.2$, at $\xi = 1.014$, and at $\eta = 0.433$. Note that this point is on the upper side of the ellipse. A small separated region, S, can be seen in this figure [8].

Goldstein and Rosenhead [3] calculated the separation over a 6 : 1 ellipse at 7° angle of attack using boundary layer theory. They find that separation starts at a very small time and that it first occurs below the rear stagnation point. Telionis

and Tsahalis [20] obtain essentially the same results as Goldstein and Rosenhead. It should be pointed out that in these two studies the rear stagnation point is constrained by the outer potential flow to remain at the location prescribed by potential flow without circulation. This unrealistic constraint results in very large adverse pressure gradients below the rear stagnation point, hence, early separation there.

Figure 8 shows streamlined contours at $t = 1.5$ computed by the Green function method. At this time the rear stagnation point is at $\xi = 1.300$ and $\eta = -0.15$.

The coefficients of lift and drag are shown in Fig. 10. Initially, both lift and drag are very large, tending to infinity as $t \to 0$. The large values of C_{DS} are due to the large surface vorticity (same as for cylinder). The large initial values of C_{DP} and C_{LP} are consistent with the expressions of Phillips [27],

$$F_\xi = -\frac{d}{dt}\int_A \rho\omega\eta \, dA,$$
$$F_\eta = \frac{d}{dt}\int_A \rho\omega\xi \, dA. \tag{44}$$

It should be emphasized that the initial large values of lift are due to the unsteadiness following the impulsive motion and are not due to circulation. Howarth [15],

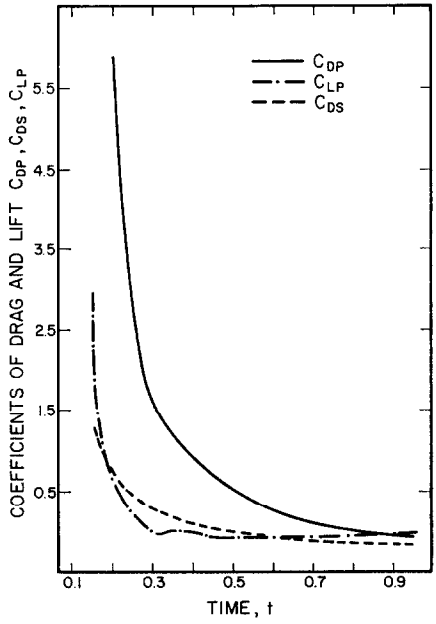

FIG. 10. Time variation of coefficients of lift and drag (2:1 ellipse at $A = 20°$).

speculating that circulation would be zero until separation starts, predicted that following an impulsive start the lift would be zero for some period and would then gradually increase.

Taneda [23] kindly agreed to carry out an experimental investigation of the ellipse problem that we computed; i.e., the initial motion over a 2 : 1 ellipse at an angle of attack of 20° (his Reynolds number is 3500). He reports large values of lift following an initial motion which is a reasonable approximation to an impulsive start. Taneda's experiments also show the gradual downward movement of the rear stagnation point.

A comparison of computation time for the two methods used can be misleading since in the Green function method computation time is independent of Δt while in the overrelaxation method it increases with increasing Δt and with decreasing residue requirements (i.e., the difference of the function at two successive iterations divided by the latest value). As an example for the flow past an ellipse, the overrelaxation method with a maximum residue of 10^{-4} took 20 minutes to compute the flow from $t = 1.0$ to 1.5 using 50 time steps. The corresponding computation time with Green's function was 28 minutes. The computations were carried out on a Univac 1108.

5. Conclusion

A numerical computation method using Green's function was developed and successfully carried out. The main advantages of this method are: (i) No outer boundary conditions are required, (ii) the field of computation is reduced, (iii) the computation time of the stream function equation does not depend on Δt, and (iv) the surface pressure distribution appears more accurate (single valued) than that obtained from the second-order successive overrelaxation method.

The computations concentrated on the flow field following an impulsively started motion. Initially both skin friction and pressure drag are very large for both the circular cylinder and the ellipse. In the case of the ellipse the initial lift is also very large. Circulation is initially zero and it gradually increases as the rear stagnation point moves down the ellipse. Separation starts at a relatively large time on the upper part of the ellipse. The computed results qualitatively agree with recent experiments of Taneda.

References

1. J. F. Thompson, Jr., S. P. Shanks, and J. C. Wu, Numerical solutions of the three-dimensional Navier–Stokes equations about a finite body, *in* "Proc. AIAA Computational Fluid Dynamics Conf., Palm Springs, Calif. July 19–20, 1973," p. 7.

2. H. BLASIUS, Grenzschichten in Flüssigkeiten mit Kleiner Reibung, *Zeit. Math. Phys.* **56** (1908), 1–37.
3. S. GOLDSTEIN AND L. ROSENHEAD, Boundary layer growth, *Proc. Cambridge Phil. Soc.* **32** (1936), 392–401. Also "Modern Developments in Fluid Dynamics," Vol. I (S. Goldstein, Ed.), Dover, New York, 1965.
4. E. J. WATSON, "Boundary-Layer Growth," *Proc. Roy. Soc., Ser. A* **231** (1955), 104–116.
5. I. PROUDMAN AND K. JOHNSON, Boundary layer growth near a rear stagnation point, *J. Fluid Mech.* **12** (1962), 161–168.
6. C. Y. WANG, The flow past a circular cylinder which is started impulsively from rest, *J. Math. Phys.* **46** (1967), 195–202.
7. C. Y. WANG, A note on the drag of an impulsively started circular cylinder, *J. Math. Phys.* **47** (1968), 451–455.
8. W. M. COLLINS AND S. C. R. DENNIS, The initial flow past an impulsively started circular cylinder," *Quart. J. Mech. Appl. Math.* **26** (1973), 53–75.
9. W. M. COLLINS AND S. C. R. DENNIS, Flow past an impulsively started circular cylinder, *J. Fluid Mech.* **60** (1973), 105–127.
10. R. B. PAYNE, Calculations of unsteady viscous flow past a circular cylinder, *J. Fluid Mech.* **4** (1958), 81–86.
11. J. S. SON AND T. J. HANRATTY, Numerical solution for the flow around a cylinder at Reynolds number 40, 200 and 500, *J. Fluid Mech.* **35** (1969), 369–386.
12. M. KAWAGUTI AND P. JAIN, Numerical study of a viscous fluid past a circular cylinder, *J. Phys. Soc. Japan* **21** (1966), 2055–2062.
13. D. C. THOMAN AND A. A. SZEWCZYK, Numerical solution of time dependent two dimensional flow of a viscous incompressible fluid over stationary and rotating cylinder, *High Speed Computing in Fluid Dynamics. Physics of Fluids Suppl. II* (1969), 76–86.
14. P. C. JAIN AND K. S. RAO, "Numerical solution of unsteady viscous incompressible fluid flow past a circular cylinder, *High Speed Computing in Fluid Dynamics. Physics of Fluids Suppl. II* (1969), 57–64.
15. L. HOWARTH, Note on the development of the circulation around a thin elliptic cylinder, *Proc. Cambridge Phil. Soc.* **31** (1939), 528.
16. C. Y. WANG, Separation and stall of an impulsively started elliptic cylinder, *Trans. ASME, J. Appl. Mech.*, December (1967), 823–828.
17. S. C. R. DENNIS AND A. STANIFORTH, Numerical method for calculating the initial flow past a cylinder in a viscous fluid, *in* "Proc. Second Internat. Conf. on Numerical Methods in Fluid Dynamics, Sept. 15–19, 1970, University of California, Berkeley" (Maurice Holt, Ed.), Springer/Verlag, Berlin, Heidelberg, New York.
18. H. J. LUGT AND H. J. HAUSSLING, Laminar flow past an abruptly accelerated elliptic cylinder at 45° incidence, *J. Fluid Mech.* **65** (1974), 711–734.
19. U. B. MEHTA AND Z. LAVAN, Starting vortex, separation bubbles and stall, a numerical study of laminar unsteady flow around an airfoil, *J. Fluid Mech.* **67** (1975), 227–257.
20. D. P. TELIONIS AND D. T. TSAHALIS, Unsteady laminar separation over cylinder started impulsively from rest, Dept. of Engineering Science and Mechanics, College of Engineering, Virginia Polytechnic Institute and State University, VPI-E-73-29, November, 1973.
21. M. SCHWABE, Über Druckermittlung in der nichtstationären ebenen Strömung, *Ingen. Arch.* **6** (1935), 34–50.
22. H. HONJI AND S. TANEDA, Unsteady flow past a circular cylinder, *J. Phys. Soc. Japan* **27** (1969), 1668–1677.
23. S. TANEDA, The development of the lift of an impulsively started elliptic cylinder at incidence, *J. Phys. Soc. Japan* **33** (1972), 1706–1711.

24. L. M. MILNE-THOMPSON, "Theoretical Hydrodynamics," 4th ed., Macmillan, New York, 1962.
25. L. V. KANTĂROVICH AND V. I. KRYLOV, "Approximate Methods of Higher Analysis," Interscience, New York, 1964.
26. L. C. WOODS, A note on the numerical solution of fourth-order differential equations, *Aero-Quart.* **5** (1954).
27. O. M. PHILLIPS, The intensity of Aeolian tones, *J. Fluid Mech.* **1** (1956), 607–624.